

1 **Local differences in neuronal activation level decorrelate spatially coherent**
2 **global fluctuations in gamma rhythms**

3 **Kaushik J. Lakshminarasimhan^{1,2}, Nikos K. Logothetis^{1,3}, Georgios A. Keliris^{1,4,5}**

4 ¹ Max-Planck Institute for Biological Cybernetics, Tübingen 72076, Germany

5 ² Dept. of Neuroscience, Baylor College of Medicine, Houston, TX 77030, USA

6 ³ Centre for Imaging Sciences, University of Manchester, Manchester M13 9PT, UK

7 ⁴ Bernstein Center for Computational Neuroscience, Tübingen 72076, Germany

8 ⁵ Bio-Imaging Lab, University of Antwerp, Universiteitsplein 1, 2610 Wilrijk, Belgium

9 **Corresponding author**

10 Georgios A. Keliris, Email: georgios.keliris@tuebingen.mpg.de

11 **Abstract**

12 Neuronal coherence is thought to constitute a unique substrate for information transmission
13 distinct from firing rate. However, since the spatial scale of extracellular oscillations typically
14 exceeds that of firing rates, it is unclear whether coherence complements or compromises the
15 rate code. We examined responses in the macaque primary visual cortex and found that
16 fluctuations in gamma-band (~40Hz) neuronal coherence correlated more with firing rate than
17 oscillations in the local-field-potential (LFP). Although the spatial extent of LFP rhythms was
18 broader, that of neuronal coherence was indistinguishable from firing rates. To identify the
19 mechanism, we developed a statistical technique to isolate the rhythmic component of the
20 spiking process and found that above results are explained by an activation-dependent increase in
21 neuronal sensitivity to gamma-rhythmic input. Such adaptive changes in sensitivity to rhythmic
22 inputs might constitute a fundamental homeostatic mechanism that prevents globally coherent
23 inputs from undermining spatial resolution of the neural code.

24 Sensory neurons often exhibit changes in coherence in addition to firing rates, providing distinct
25 substrates for representing information. Although the precise behavioral consequences of
26 differences in the timescales of these two codes continue to be debated¹⁻³, recent work suggests
27 that they may operate in parallel to constitute a multiplexed temporal code⁴. A related but often
28 overlooked issue is the compatibility of their spatial scales. Whereas spatially correlated firing is
29 detrimental to the information capacity of rate codes, it is a defining aspect of synchrony-based
30 codes. Entrainment of spikes from distinct columns can undermine the spatial resolution of the
31 representation established by differences in firing rates.

32 Neuronal coherence in the gamma frequency range (30-90 Hz) is ubiquitous in the
33 mammalian brain and has been implicated in a variety of functions including sensory
34 processing⁵⁻⁷, attentional selection^{8,9}, perceptual modulation^{10,11}, working memory¹², memory
35 encoding and retrieval¹³ as well as neurological disorders like Schizophrenia and Parkinson's
36 disease^{14,15}. Gamma oscillations are thought to be generated locally within the cortical
37 microcircuit^{16,17} and have been reported to span hundreds of micrometers in the macaque brain.
38 How does the spatial extent of gamma-band coherence compare to that of firing rates? What
39 mechanisms, if any, help prevent global fluctuations in rhythms from compromising the integrity
40 of the columnar organization?

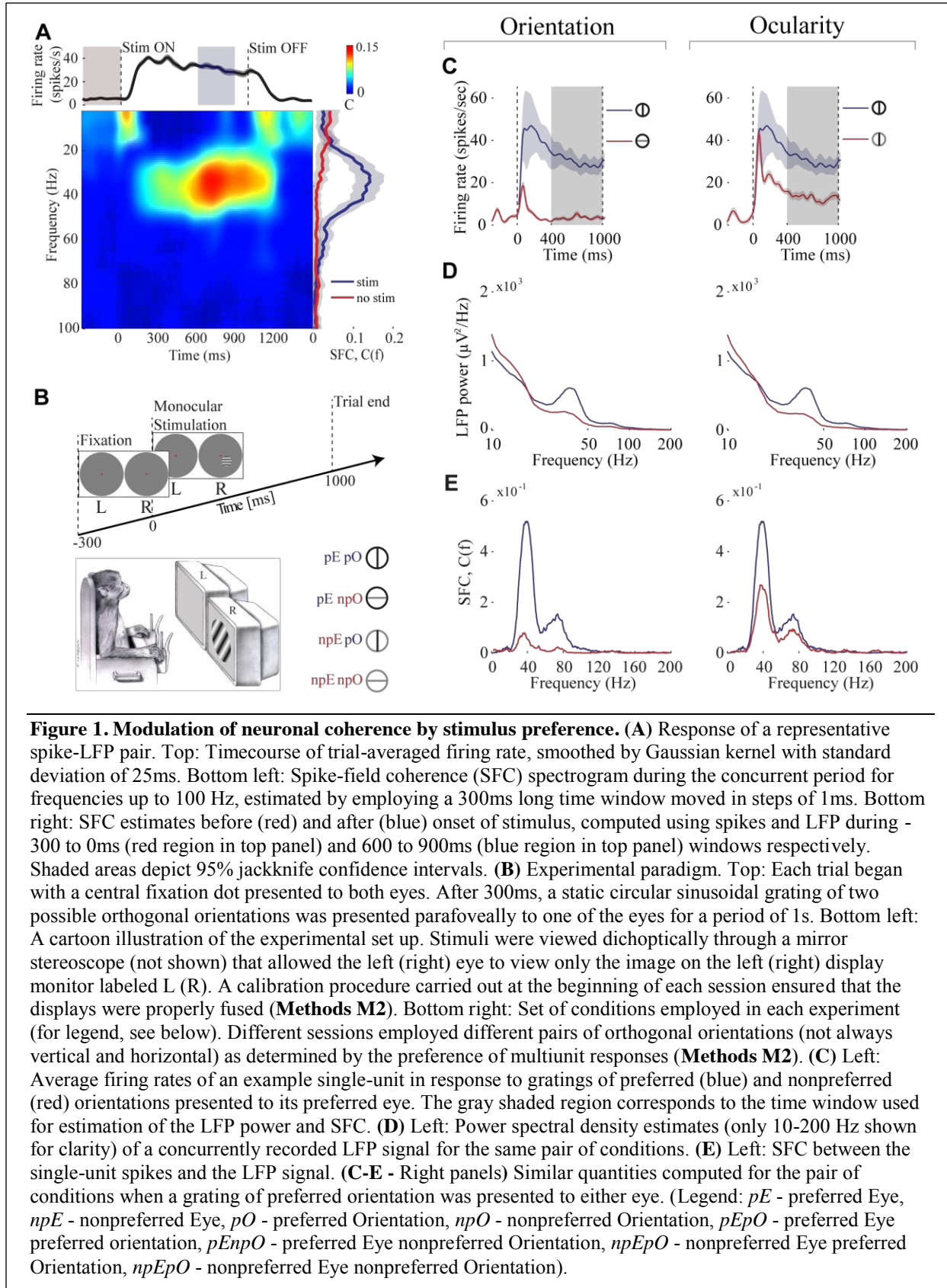
41 To address these questions, we used multi-tetrode recordings to examine concurrent
42 changes in spiking activity of single-units, local field potentials (LFP), and spike-field coherence
43 (SFC) in the primary visual cortex of two rhesus macaques viewing monocularly presented
44 gratings. Since the average synaptic activity is thought to be a major source of fluctuations in the
45 LFP¹⁸⁻²⁰, we expected the strength of LFP oscillations to best predict changes in the extent of
46 synchronous firing estimated using SFC. In contrast, we found that gamma-band SFC was
47 correlated more strongly with firing rate than strength of gamma rhythms in the LFP. We probed
48 the underlying mechanism by partitioning the spiking process into two components – an
49 asynchronous component that reflected stimulus-dependent changes in activation level, and a
50 synchronous component driven by gamma oscillations in the LFP. We found that sensitivity of
51 neurons to synchronous drive increased significantly with mean activity, and these changes
52 specifically contributed to the stronger correlations between neuronal synchrony and firing rates.
53 Such activity-dependent changes in sensitivity might constitute a fundamental mechanism that
54 preserves the spatial resolution of the neural code by selectively entraining only highly activated
55 neurons thus effectively decorrelating global, non-specific fluctuations in gamma rhythms.

56 **Results**

57 **Single-unit spike-field coherence (SFC) in the gamma band**

58 We recorded from 474 sites from two macaque monkeys viewing monocularly presented grating
59 stimuli (**Methods M1 & M2**). A total of 811 single-units were isolated, among which ~75%
60 ($n=610/811$) were deemed visually responsive (**Methods M3**). For each responsive unit,
61 neuronal coherence was assessed by estimating spike-field coherences (SFC) between their spike
62 trains and concurrently recorded field potentials (LFP) (**Methods M3 – Equation 1**). The
63 response of a representative single-unit is shown in **Figure 1A**. The onset of the stimulus is
64 accompanied by a sharp transient increase in the firing rate followed by a period of relatively
65 sustained firing. As seen from the spike-field coherogram, there was a significant increase in
66 coherence in the gamma range (30-45 Hz) following stimulus onset and this was most
67 pronounced during the sustained period of neuronal firing (400-1000ms). Therefore, we confined
68 all our analyses to this time window. Stimulus-evoked spiking activities of approximately 27%

69



70 of visually responsive units ($n=166/610$; 119 from monkey D98; 47 from monkey F03) were
71 found to exhibit significant gamma-band SFC ($p<0.01$; permutation test, **Methods M3**). SFCs
72 were estimated between spike trains of the above single-units and LFPs measured from each of
73 the simultaneously recorded sites (up to 6 sites in chronic; 4 sites in non-chronic recordings),
74 yielding a total of 400 spike-LFP pairs. Since we want to study the fluctuations in gamma-band
75 coherence, following results pertain to these 400 spike-LFP pairs unless stated otherwise.

76 **Stimulus-dependent changes in SFC are correlated with firing rates and LFP**

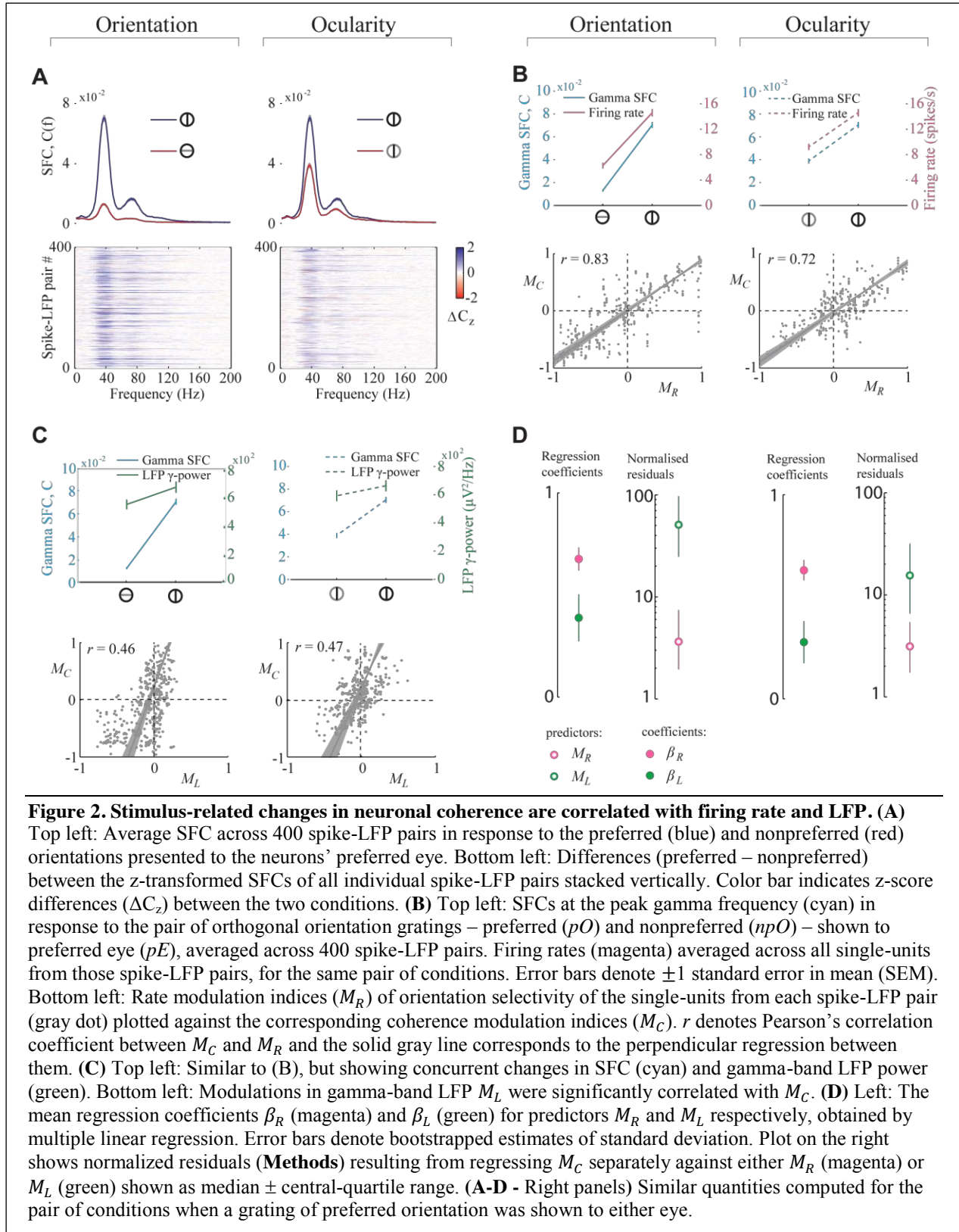
77 We first analyzed stimulus-induced changes in SFC that accompany changes in firing rate and
78 LFP for each spike-LFP pair by comparing responses under two sets of stimulus conditions (**Fig.**
79 **1B**): (1) the pair of conditions when either the preferred or nonpreferred orientation was
80 presented to the neuron's preferred eye ($pEpO$ vs $pEnpO$), and (2) the pair of conditions when
81 the preferred orientation was presented to either the preferred or nonpreferred eye separately
82 ($pEpO$ vs $npEpO$). These set of conditions were chosen to capture any effects that the differences
83 in spatial scales between orientation and ocular columns might bear on our analyses.

84 We found that across the population of all spike-LFP pairs, changes in neuronal firing
85 rate and gamma-band SFC were concomitant. Stimuli that elicited an increase in firing also
86 produced higher SFC in most cases, i.e. degree of entrainment of spike trains to gamma-band
87 LFP increased with spike density. On average, this was true both when neuronal response was
88 manipulated by changing grating orientation as well as eye. As illustrated for one representative
89 spike-LFP pair, increased spiking activity in response to the neuron's preferred stimuli (**Fig. 1C**)
90 is accompanied by an increase in LFP power around 40 Hz in a neighboring site (**Fig. 1D**).
91 Moreover, this spike-LFP pair also exhibits an increased SFC in this frequency range (**Fig. 1E**).

92 Similar effects were observed in the majority of all analyzed spike-LFP pairs and are
93 readily noticed in the population average of SFCs (**Fig. 2A, Supplementary Fig. 2A**), firing
94 rates (**Supplementary Figures 1A,2B**), and LFP power spectra (**Supplementary Figures**
95 **1B,2C**). We tested the significance of stimulus-dependent changes in SFC (C) at the peak
96 gamma frequency and firing rates (R) across the population of all spike-LFP pairs and found that
97 both quantities increased significantly in response to the neuron's preferred orientation as well as
98 preferred eye (**Fig. 2B** – top panels; population rate: $R_{pEpO}=14.7\pm 0.8$ spikes s^{-1} ; $R_{pEnpO}=7.0\pm 0.6$
99 spikes s^{-1} ; $R_{npEpO}=9.1\pm 0.7$ spikes s^{-1} , and population coherence: $C_{pEpO}=0.070\pm 0.002$;
100 $C_{pEnpO}=0.013\pm 0.001$; $C_{npEpO}=0.039\pm 0.002$; $p<10^{-10}$; Wilcoxon rank-sum test for the difference in
101 medians between preferred and non-preferred responses). We examined the relationship between
102 changes in firing rates and SFCs across the population, by comparing coherence modulation
103 indices M_C against corresponding rate modulation indices M_R (**Methods M3 – Equation 2**).
104 There was a strong positive correlation between M_C and M_R for the set of orientation (**Fig. 2B** –
105 bottom left; Pearson's correlation $r=0.83$; $p<10^{-10}$) as well as ocularity conditions (**Fig. 2B** –
106 bottom right, **Supplementary Figure 2D**; $r=0.72$; $p<10^{-10}$). The above relationships were
107 quantified using perpendicular regression and the slopes were found to be close to unity for the
108 pair of orientation conditions ($M_C\approx 0.88M_R$; 95% confidence interval (CI): slope=[0.83 0.93]) as
109 well as for ocularity ($M_C\approx 0.87M_R$; 95% CI: slope=[0.82 0.93]) suggesting that modulation in
110 gamma-band synchrony and firing rate tend to be nearly identical.

111 Next, we examined whether changes in SFC are related to changes in the strength of
112 gamma-band LFP. If LFP primarily reflects the average synaptic input to neurons in the local
113 circuit, then an increase in gamma-band power of the LFP should predict an increase in the
114 extent of coherent firing of those neurons. Indeed, stimulus-related modulations of SFC were

115



116 largely congruent (**Fig. 2C** - top panels) and significantly correlated with those of the LFP
117 gamma-band power M_L in both pairs of stimulus conditions (**Fig. 2C** – bottom panels,
118 **Supplementary Figure 2E**; orientation: $r=0.46$; $p<10^{-10}$; ocularity: $r=0.47$, $p<10^{-10}$).
119 Surprisingly however, these correlations were significantly smaller in magnitude than their
120 correlation with firing rate ($p<10^{-10}$, one-tailed two-sample t -test for the difference in
121 correlations). Since majority of spike-LFP pairs were comprised of spikes and LFPs recorded at
122 different sites, we wanted to know whether weaker correlation of neuronal coherence with LFP
123 was due to distance effects. We tested this by grouping spike-LFP pairs based on the electrode
124 separation between singleunit spikes and LFPs. We found that the correlation coefficients were
125 not significantly different across groups thus ruling out this possibility (**Supplementary Fig. 3**).

126 To further quantify the differences between the effect of firing rate and strength of
127 gamma-band LFP on neuronal coherence, we performed a multiple linear regression of M_C with
128 both M_R and M_L as simultaneous predictors (**Methods M3 – Equation 3**). We found that the
129 regression coefficients on M_R were significantly larger than on M_L (**Fig. 2D** ; Orientation:
130 $\beta_R=0.68\pm0.06$, $\beta_L=0.39\pm0.1$, $p<10^{-10}$, Ocularity: $\beta_R=0.63\pm0.05$, $\beta_L=0.29\pm0.1$, $p<10^{-10}$; one-tailed
131 t -test comparing regression coefficients β_R vs β_L), indicating that changes in firing rate rather
132 than LFP, better explained the stimulus-related variability in gamma-band coherence. In fact,
133 changes in SFC predicted by a linear regression model solely with M_R as predictor generated
134 residuals that were about five to ten times smaller ($p<10^{-5}$, t -test) than those predicted using M_L
135 alone (**Fig. 2D**). Nevertheless, regression coefficients of the two predictors were significantly
136 above zero implying that firing rate and the strength of LFP oscillations both carried independent
137 information about changes in neuronal coherence.

138 Above results demonstrate that changes in SFC are correlated both with firing rate and
139 gamma-band LFP, when those changes were induced by stimulus manipulation (either the
140 orientation or the eye). To test whether these quantities are also correlated in the absence of
141 stimulus change, we computed their correlated variability across trials within each stimulus
142 condition. To do this, we estimated the correlation between trial-by-trial pseudo-SFC (pSFC)
143 values (**Methods M3 – Equation 4**) and concomitant fluctuations in firing rate (ρ_{RC}) as well as
144 gamma-band LFP power (ρ_{LC}) at all frequencies. If correlations were exclusively due to stimulus
145 change, one would expect them to vanish when the measurements are conditioned on the
146 stimulus. In contrast, across the population of all spike-LFP pairs, both ρ_{RC} and ρ_{LC} were found
147 to be significantly positive in the gamma-band ($p<10^{-3}$, Fisher's combined probability test)
148 within each stimulus condition (**Supplementary Fig. 4A, B**). Thus correlations persisted in the
149 absence of stimulus change. Furthermore, the strength of correlation at the peak gamma
150 frequency was found to depend on stimulus identity such that stronger input drive elicited greater
151 correlations ($pEpO > npEpO > pEnpO$; $p<10^{-5}$, Kruskal-Wallis test for correlations vs stimulus).
152 Specifically, presentation of the neurons' preferred stimuli increased the correlation between
153 neuronal synchrony and firing rate (**Supplementary Fig. 4A** – inset; ρ_{RC} : $pEpO$ - 0.16 ± 0.01 ,
154 $npEpO$ - 0.13 ± 0.01 , $pEnpO$ - 0.11 ± 0.01), as well as the correlation between synchrony and
155 gamma-band LFP (**Supplementary Fig. 4B** – inset; ρ_{LC} : $pEpO$ - 0.15 ± 0.01 , $npEpO$ - 0.10 ± 0.01 ,
156 $pEnpO$ - 0.04 ± 0.01). These results have two key implications. First, correlation between firing
157 rate, LFP and neuronal coherence is not simply due to these quantities all being identically tuned
158 to stimulus, but is likely a signature of an intrinsic mechanism that couples changes in firing rate
159 and gamma-band LFP to neuronal coherence. Second, this mechanism might be sensitive to
160 stimulus drive such that a stronger drive leads to a tighter relationship between these measures.

161

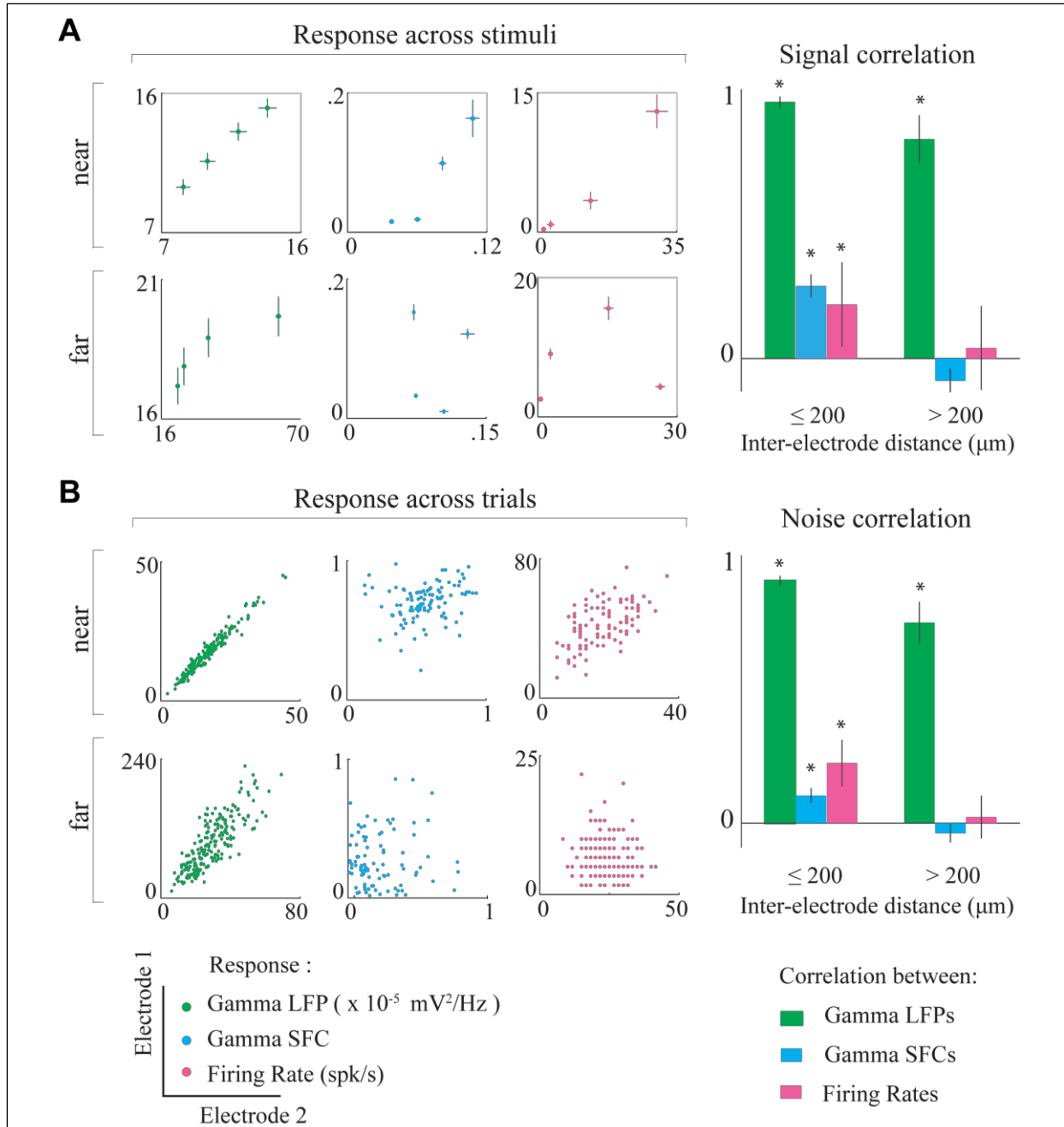


Figure 3. Spatial scales of LFP and coherence. (A) Left: Trial-averaged responses to four different stimuli (see Fig. 1B) recorded at two pairs of example sites that were nearby (top panels) or far away (bottom panels). Whereas gamma-band LFP power, gamma-band SFC, and firing rates were all similarly tuned across nearby sites, only gamma-band LFP was similar across more distant sites. Right: Average signal correlations between pairs of nearby (<200 μm) and distant (>200 μm) sites for each of the three response measures. Whereas the tuning of gamma-band LFP remained significantly correlated between distant sites, those of SFC and firing rate were not significantly different from zero for distant sites. (B) Left: Trial-by-trial responses to one of the stimuli at two pairs of example sites. Unlike LFP oscillations, fluctuations in SFC and firing rates were uncorrelated at the pair of distant sites. Right: Average noise correlations showed similar distant-dependent effects as signal correlations. Error bars denote ± 1 SEM (* $p < 0.01$, two-sided sign test for median correlation of zero).

162 **Neuronal coherence and LFP are spatially dissociated**

163 Why do firing rates, rather than LFP rhythms, better predict changes in neuronal coherence? We
164 have previously shown that, for stimuli presented within the classical receptive field, LFP
165 reflects activity spanning the order of ocular dominance columns²¹. Since coherence was more
166 correlated with firing rate, we hypothesized that changes in the global strength of rhythmic
167 synaptic input reflected in the LFP must be gated by mechanisms of a spatially local origin to
168 ultimately limit the spatial extent of synchronous firing. If this is true, then the spatial scale of
169 neuronal synchrony would be determined primarily by that of the firing rate code, and would
170 hence be much smaller than the scale of LFP rhythms.

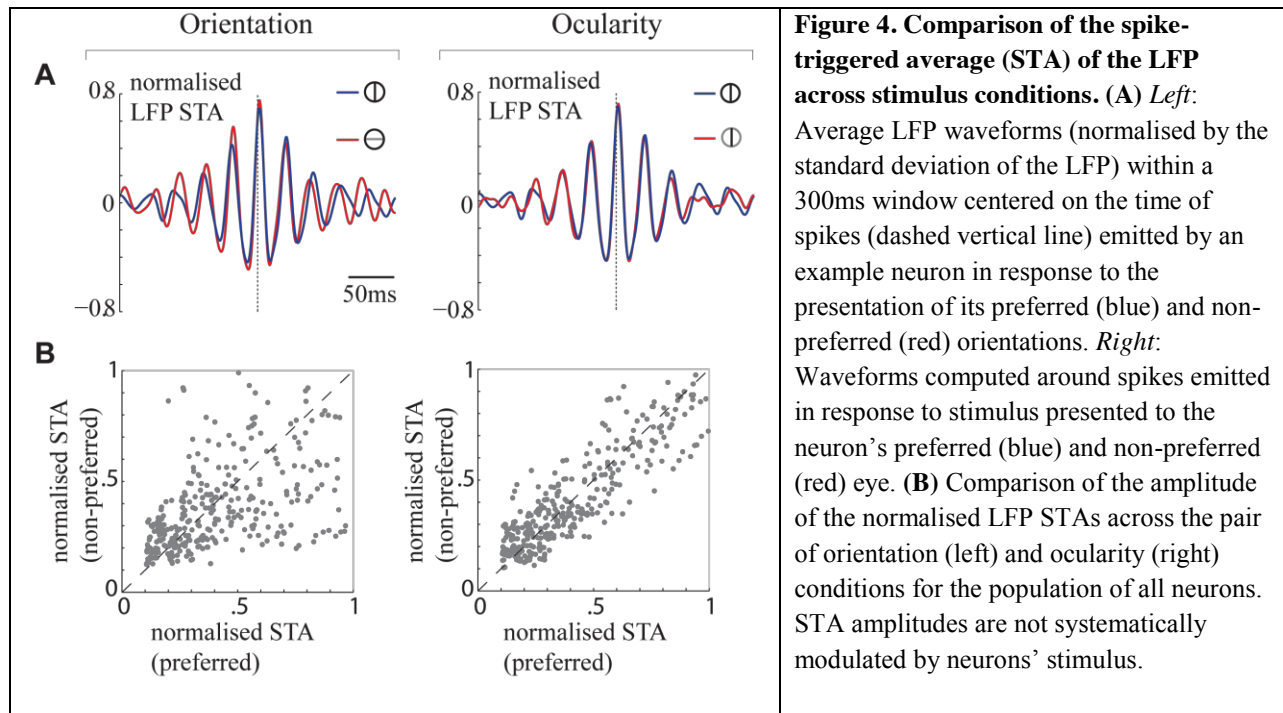
171 To test this, we estimated the pairwise correlation between SFCs of simultaneously
172 recorded neurons as a function of the distance between electrodes from which the neurons were
173 recorded (**Fig. 3**, cyan). Likewise, we also estimated correlated variability in firing rates of all
174 pairs of neurons (**Fig. 3**, magenta) as well as correlations in gamma-band LFP powers at the
175 respective electrode sites from which those neuronal pairs were recorded (**Fig. 3**, green). In each
176 case, we computed both stimulus-induced (also called ‘signal correlation’, **Fig. 3A**) and
177 stimulus-independent (‘noise correlation’, **Fig. 3B**) components of the correlation. To assess the
178 effect of spatial separation, we analysed how correlations in each of the three measures (gamma
179 LFP, firing rate, and gamma SFC) changed with distance by dividing the pairs of electrodes into
180 two groups of roughly equal size: those that were nearby ($\leq 200 \mu\text{m}$) or far away ($> 200 \mu\text{m}$).

181 The panel on the left in **Figure 3A** shows concurrent stimulus-induced changes in
182 gamma-band LFP (green), SFC (cyan), and firing rate (magenta) at pairs of nearby (top) and far
183 away (bottom) electrode sites. Whereas signal correlations between gamma-band LFPs were
184 high at both pairs of locations, correlations in SFC and firing rates were both only significant
185 between neurons in nearby sites. This trend was observed across our dataset (**Fig. 3A** - right).
186 The similarity in tuning of gamma-band LFP power remained large and significantly above zero
187 across long distances (nearby pairs: $r=0.95\pm 0.04$, $p<10^{-10}$, two-sided sign test; distant pairs:
188 $r=0.81\pm 0.18$, $p<10^{-10}$), whereas signal correlations in both SFCs (nearby pairs: $r=0.27\pm 0.06$,
189 $p<10^{-10}$; distant pairs: $r=-0.08\pm 0.06$, $p=0.053$) and firing rates (nearby pairs: $r=0.2\pm 0.15$,
190 $p=0.0015$; distant pairs: $r=0.04\pm 0.16$, $p=0.23$) were only significant between neuronal pairs in
191 nearby sites. The magnitude of noise correlations exhibited a similar trend (**Fig. 3B**). Significant
192 correlations were found between trial-by-trial changes in gamma LFP regardless of distance
193 (nearby pairs: $r=0.90\pm 0.03$; distant pairs: $r=0.75\pm 0.16$). On the other hand, SFCs (nearby pairs:
194 $r=0.10\pm 0.05$; distant pairs: $r=-0.04\pm 0.04$) and firing rates (nearby pairs: $r=0.22\pm 0.08$; distant
195 pairs: $r=0.02\pm 0.07$) of neurons at distant sites were both uncorrelated.

196 **LFP rhythms are robustly correlated with membrane potential**

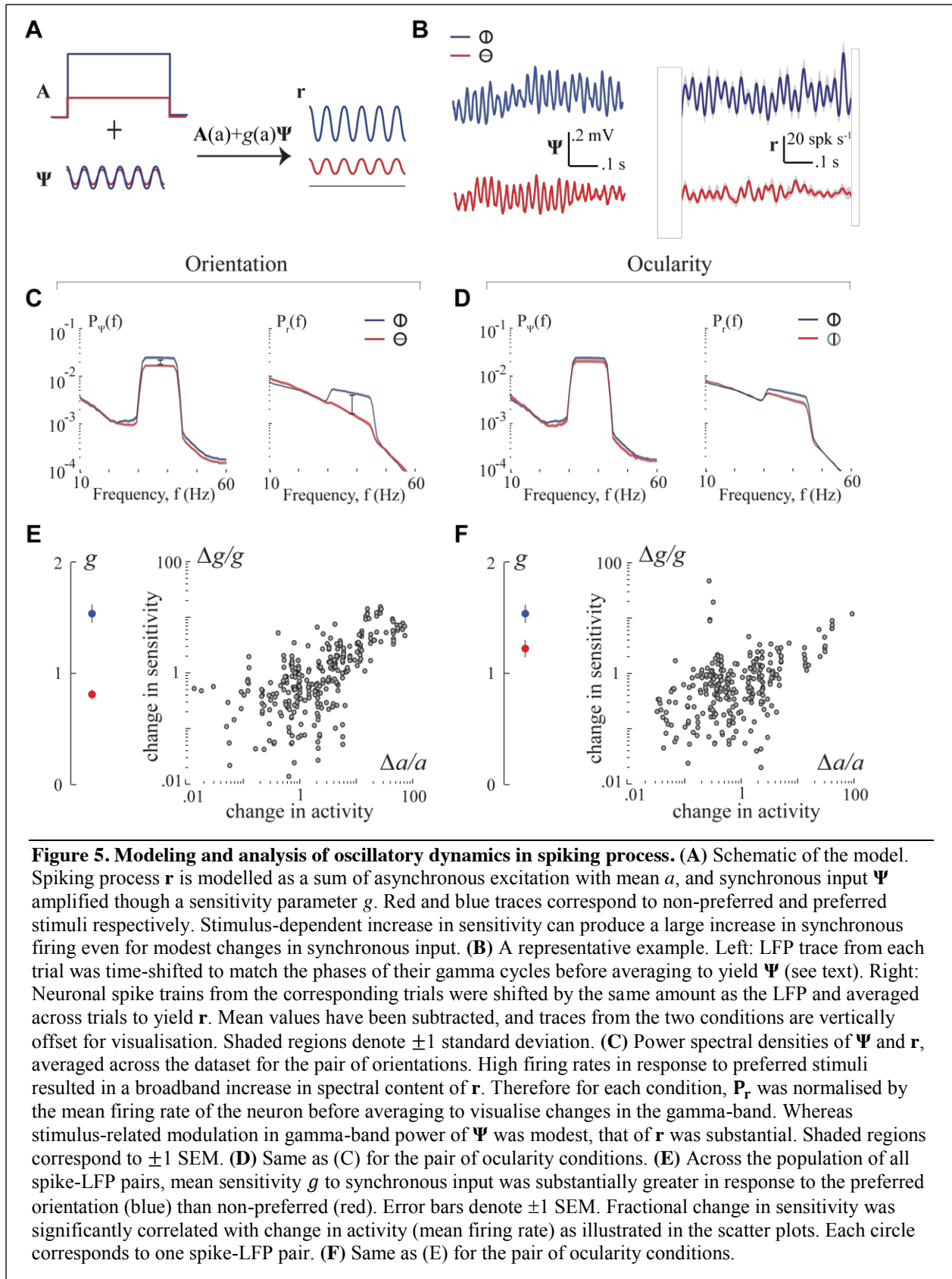
197 Above results suggest that although neurons with large separation likely receive similar rhythmic
198 synaptic inputs as implied by the long-range correlations in the LFP, their outputs are incoherent.
199 Instead the spatial scale of neuronal coherence is similar to that of firing rates. This raises the
200 possibility that globally correlated rhythmic synaptic inputs are gated by spatially local
201 mechanisms that are sensitive to neurons’ activation level, to ultimately restrict the extent of
202 rhythmic synchronization of their outputs.

203 However a alternative explanation for dissociation in the spatial scales of neuronal
204 coherence and LFP is that gamma activity in LFP does not reflect the strength of rhythmic
205 synaptic inputs to the neurons in our recording. If rhythmic input to individual neurons was more



206 local than the LFP suggests, then the lack of a strong relation between neuronal synchrony with
 207 LFP could be explained away without the need to invoke any local mechanism. A direct way to
 208 test this alternative would be to compare LFP rhythms against oscillations in membrane potential
 209 of the neurons in our dataset. Such a direct comparison was not possible due to difficulties
 210 associated with performing stable intracellular recordings in awake macaques. Instead, we
 211 indirectly estimated the correlation between membrane potential and LFP by computing spike-
 212 triggered average (STA) of the LFP. We computed normalised STAs for each neuron under all
 213 stimulus conditions by dividing the STA by the standard deviation of the LFP under the
 214 corresponding condition (**Methods M3**). A previous study involving simultaneous intra- and
 215 extracellular recordings has shown that this normalised STA is essentially equal to the cross-
 216 correlation between the neuron's membrane potential and the LFP²². Therefore we used the
 217 amplitude of the normalised STAs to assess whether gamma-band LFP is a good predictor of
 218 gamma rhythmic synaptic inputs to the individual neurons in our dataset. **Figure 4A** shows
 219 normalised LFP STAs estimated using spikes of one example neuron under the pair of
 220 orthogonal stimulus conditions. STAs of this neuron revealed a substantial correlation between
 221 the LFP and synaptic inputs in the gamma range, and the magnitude of this correlation was
 222 similar across stimulus conditions. This was true on average across the population of all neurons
 223 (STA amplitudes: *pEpO* - 0.44 ± 0.28 , *npEpO* - 0.44 ± 0.26 , *pEnpO* - 0.42 ± 0.27). The median
 224 amplitudes of STA were not significantly different across orientations of the grating (**Fig. 4B**;
 225 $p=0.50$, Wilcoxon rank-sum test) or the eyes that were stimulated (**Fig. 4B – right**; $p=0.57$). If
 226 gamma rhythmic input to individual neurons was already localized in space and varied
 227 concomitantly with firing rates, then its correlation with the global LFP signal should change
 228 with stimulus. In contrast, our results show that gamma-band LFP can predict the strength of
 229 rhythmic synaptic input equally well under all stimulus conditions. This robustness suggests that
 230 rhythmic input to neurons must be broadly correlated across space and argues for an active
 231 mechanism that decorrelates the neuronal outputs.

232



233 **Activity-dependent increase in sensitivity to synchronous input**

234 In order to account for our experimental findings, we considered a simple linear model in which
235 the spiking process \mathbf{r} is given by $\mathbf{r} = \mathbf{A} + g \cdot \boldsymbol{\psi}$ where \mathbf{A} denotes asynchronous activation with
236 mean a that reflects the net excitatory synaptic drive, $\boldsymbol{\psi}$ is the rhythmic synaptic input, and the
237 gating parameter g represents the sensitivity to synchronous input. The activation parameter a
238 determines the average firing rate of the neuron, while g determines how well synchronous input
239 $\boldsymbol{\psi}$ is encoded in the temporal pattern of spikes. In this model, rhythmic input drives coherence in
240 the output while asynchronous activation reduces it. Thus neuronal coherence should be
241 positively correlated with the strength of rhythmic input but anti-correlated with the overall
242 activation level reflected in the firing rate (**Supplementary notes, Supplementary Fig. 5A**), a
243 prediction at odds with our experimental results. However, if there is an activity-dependent
244 increase in sensitivity to synchronous input ($g \propto a$) that facilitates the transfer of synchrony,
245 synchrony at the output could increase with firing rate (**Supplementary notes, Supplementary**
246 **Fig. 5B**). Therefore, we wanted to know whether stimulus-related increase in neuronal coherence
247 in our dataset was attributable to such an increase in sensitivity to rhythmic input accompanying
248 the overall increase in activation level in response to preferred stimulus (**Fig. 5A**).

249 For each spike-LFP pair, we used the LFP signal as a proxy for $\boldsymbol{\psi}$ and inferred model
250 parameters a and g that explained the spiking activity \mathbf{r} . There were two challenges in this
251 approach. First, while average synaptic input constitutes the major source of extracellular
252 currents, LFP is also likely to contain traces of currents emerging from calcium spikes, action
253 potentials, and spike after-potentials. Since the gamma rhythmic synaptic inputs are not precisely
254 phase-locked with stimulus onset, we cannot use stimulus-locked trial-averaging to isolate the
255 component reflecting rhythmic synaptic input. Second, spikes from individual trials are typically
256 too sparse and noisy to allow reliable assessment of the underlying temporal dynamics. Once
257 again due to the lack of phase consistency between rhythmic spiking activity and stimulus onset,
258 trial-averaged firing rates typically fail to reveal the rhythmic process underlying spike
259 generation (see Fig. 1C for example). We used the following technique to overcome both issues.
260 We time-shifted our LFP traces on each trial by a small amount so that the peak gamma
261 frequency in the LFP was phase-matched across trials. Spike trains from corresponding trials
262 were shifted by the same amount to ensure that this procedure preserved the phase consistency of
263 spike-trains relative to LFP i.e. spike-field coherence (**Supplementary Fig. 6**). **Figure 5B** shows
264 the trial-averaged traces of the resulting time-shifted LFP ($\boldsymbol{\psi}$) and spiking process (\mathbf{r})
265 reconstructed above for a representative spike-LFP pair. In this example, it is clear that although
266 the increase in amplitude of gamma oscillations in $\boldsymbol{\psi}$ was modest, there was a marked increase in
267 the rhythmicity of \mathbf{r} in response to preferred stimulus. This was observed across our dataset and
268 can be noticed in the population averages of the power spectra of $\boldsymbol{\psi}$ and \mathbf{r} (**Fig. 5C, D**).

269 If sensitivity g was independent of stimulus, the relative change in spectral content of \mathbf{r}
270 would be comparable to those in $\boldsymbol{\psi}$. However, the fractional increase in gamma-band power was
271 larger in \mathbf{r} suggesting that there was a stimulus-dependent increase in sensitivity. To confirm
272 this, we fit the activation parameter a and sensitivity g individually for each spike-LFP pair.
273 Whereas a was trivially given by the mean of the spiking process \mathbf{r} , sensitivity g was inferred by
274 computing the fraction of temporal variability in spiking that was contributed by the rhythmic
275 input (**Supplementary Fig. 7, Methods equation (5)-(6)**). As shown in **Figure 5E, F** (left
276 panels), there was indeed a significant increase in sensitivity to rhythmic input in response to
277 preferred stimulus ($p < 10^{-5}$; Wilcoxon rank-sum test). Moreover, changes in sensitivity were
278 strongly correlated with the increase in neuronal activation a (Pearson's correlation - orientation:

279 $r=0.59, p<10^{-5}$; ocularity: $r=0.31, p<10^{-5}$) (**Fig. 5E, F** - right), and not to the strength of rhythmic
280 input (orientation: $p=0.78$; ocularity: $p=0.57$) (**Supplementary Fig. 8**). Does the increase in
281 sensitivity specifically underlie the increase in neuronal coherence? We tested this by
282 partitioning the spike-LFP pairs into two groups, based on whether stimulus-dependent changes
283 in neuronal coherence were congruent or incongruent with firing rates. Whereas preferred stimuli
284 elicited a large increase in sensitivity in the congruent pairs, the effect on incongruent pairs was
285 much smaller and barely approached significance (orientation: $p=0.07$, Wilcoxon rank-sum test,
286 $n=69$ spike-LFP pairs; ocularity: $p=0.09, n=100$; **Supplementary Fig. 9**) confirming that
287 decrease in coherence with firing rates in these pairs were attributable to the lack of increase in
288 sensitivity to rhythmic input. Together, these results suggest that there is activity-dependent
289 increase in sensitivity to rhythmic input, and that this specifically underlies the strong
290 correlations between firing rate and neuronal coherence.

291 **Discussion**

292 We examined concomitant changes in gamma-band neuronal coherence, firing rate, and strength
293 of extracellular gamma rhythms in the primary visual cortex of awake rhesus macaques viewing
294 monocularly presented grating stimuli. We found three key results that all point to an active
295 mechanism that modulates the transfer of synchrony by neurons depending on their overall
296 activation level.

297 First, neuronal gamma-band coherence quantified using spike-field coherence (SFC)
298 increased with firing rate such that stimulus identity (both orientation and eye) was encoded in
299 both quantities. Although neuronal coherence has previously been observed to increase with
300 firing rate, some studies have found that rate and coherence encode different features of the
301 stimulus leading to the view that the two codes carry complementary information^{23–25}. In
302 contrast, our result suggests that the two may also operate in tandem to increase information
303 throughput about the same stimulus feature.

304 Second, neuronal coherence was more strongly correlated with firing rate than with the
305 strength of gamma rhythms in the local field potential (LFP). This is surprising because gamma
306 rhythms in the LFP are thought to reflect synchronous synaptic inputs^{26,27} that orchestrate
307 rhythmic synchronization between neurons. On the other hand, SFC measures coherence in the
308 spiking activity and largely reflects the amount of coherent output of the neurons. The fact that
309 SFC was better predicted by firing rates suggests that the net coherence transferred by neurons
310 depends more strongly on their overall activation level than on the strength of synchronous input.
311 In one previous study, individual neurons in cortical slices were stimulated by injecting current
312 steps of different means combined with noisy gamma oscillatory currents to study how the
313 oscillations interact with the overall activation level²⁸. The authors observed that the activation
314 level had a significant impact on the timing of spikes elicited by gamma oscillatory input in a
315 manner that increased the probability of coincidental spiking between neurons with similar firing
316 rates, a phenomenon they called “rate-specific synchrony”. Although their work does not pertain
317 to oscillatory neuronal synchronization and therefore distinct from ours, it supports the notion
318 that activation level could have a significant impact on determining how gamma oscillatory input
319 affects neuronal spiking.

320 Third, the spatial scale of gamma-band neuronal coherence was much smaller than
321 extracellular gamma rhythms, but indistinguishable from that of the firing rate code. If coherent
322 spiking were a consequence of passive integration of rhythmic synaptic inputs reflected in the
323 LFP, it would share the same spatial scale as extracellular rhythms. The fact that the spatial
324 correlation of neuronal coherence was instead comparable to that of firing rates reinforces the
325 view that neuronal activation level must play a key role in the gating of rhythmic inputs. It
326 follows that the local differences in activation level would decorrelate long-range coherent
327 fluctuations in gamma rhythmic synaptic input to restrict the spatial scale of coherence in spiking
328 activity. Although the spatial scale of LFP gamma rhythms in our measurements is consistent
329 with earlier work, it has been shown that this scale is in fact variable and depends on the size of
330 the stimulus^{29,30}. While it is likely that the precise scale of extracellular rhythms in our dataset is
331 specific to our choice of stimulus size, we believe this does not affect our interpretation. In fact,
332 large spatial correlations in LFP rhythms induced by our stimulus helped capture the decoupling
333 between the spatial scale of neuronal coherence and the LFP. We note that the pattern of results
334 was qualitatively similar regardless of whether changes in responses were brought about by
335 changes in orientation or ocularity. Given that the spatial scale of orientation and ocular columns
336 in macaque V1 differ by at least an order of magnitude^{31,32}, our findings here are likely to extend

337 beyond the encoding of specific stimulus features. Together, our experimental results all point to
338 some form of interaction between neuronal activation-level and gating of rhythmic inputs.

339 We tested this possibility by developing a novel statistical technique to fit a linear model
340 that explicitly captured the dependence of rhythmic spiking on both the overall activation level
341 as well as the strength of synchronous input through a sensitivity parameter. We found that
342 stimulus-related increase in gamma rhythmicity of the spiking process could not be entirely
343 accounted for by an increase in strength of rhythmic synaptic input but stemmed largely from an
344 activation-dependent increase in neuronal sensitivity to rhythmic drive. Although our model is
345 phenomenological, past experiments suggest that our findings may have mechanistic origins at
346 the neuronal level. Intracellular recordings in vivo have demonstrated an activity-dependent
347 increase in spike threshold that facilitates coincidence detection³³⁻³⁷. Consistent with this,
348 biophysical modeling studies and slice recordings show that increase in Poisson-like synaptic
349 background activity increases the sensitivity of pyramidal neurons to temporally structured
350 synaptic input³⁸⁻⁴⁰ by effectively increasing voltage threshold via *M* currents^{41,42}. It is possible
351 that such dynamic changes in synaptic integration properties may also underlie the ability of
352 neurons to adapt their sensitivity to gamma rhythms reported here. In fact, recently Perrenoud et
353 al used intracellular recordings to demonstrate that increased phase-locking of pyramidal neurons
354 to the gamma cycle is facilitated by an overall increase in the average membrane potential in
355 response to visual stimulation⁴³. Alternatively, the observed changes in response characteristics
356 of neurons and the associated gamma-band synchronization could be a reflection of network-
357 level computations such as divisive normalization⁴⁴. If this is the case, the normalization pool is
358 likely to be confined to within an orientation column for otherwise we would not have observed
359 orientation-dependent changes in neuronal sensitivity. Further experiments will be necessary to
360 identify whether the observed phenomenon is dominated by a cellular or network mechanisms.

361 There are some fundamental issues in relation to past findings which merit further
362 scrutiny. First, increase in neuronal gamma-band synchronization with firing rate has been
363 reported previously^{5,6,12,45,46}. Theoretical studies have shown that this dependence is expected for
364 a broad class of statistical models^{47,48}. Mechanistically, such dependence could stem from a
365 simple threshold nonlinearity in the neurons⁴⁹. However, simulations of model neurons with a
366 fixed threshold substantially underestimated the magnitude of rate-dependent increase in SFC
367 observed in our data (**Supplementary Fig. 10-11**). Instead, our data was better explained by a
368 model in which neuronal threshold increased with the mean activity of the neurons
369 (**Supplementary Fig. 12**). This dynamic threshold model is consistent with several past
370 experimental results, and supports the idea that the mechanism mediating neuronal coherence is
371 sensitive to neuronal activation. Second, since synaptic currents constitute a major source of
372 fluctuations in the LFP¹⁸⁻²⁰, we used gamma oscillatory power in the LFP as a proxy for the
373 strength of rhythmic synaptic input to neurons. Although the precise magnitude of rhythmic
374 input to individual neurons likely differs from that estimated using the LFP²⁰, our conclusions
375 are valid insofar as the relative changes in LFP oscillations are correlated with those of
376 oscillatory input to single neurons across stimulus conditions. It is difficult to test this precisely
377 without intracellular recordings. However it has previously been shown that the average LFP
378 waveform around the time of a neuron's action potential (spike-triggered LFP) reflects the
379 correlation between the LFP and that neuron's synaptic inputs²². The STAs in our dataset had
380 particularly large gamma-band powers and their amplitudes were not significantly modulated by
381 stimulus, so we believe gamma activity in the LFP provided a robust readout of the strength of
382 gamma rhythmic synaptic inputs. Finally, neuronal coherence in the gamma band is known to

383 vary independently of firing rates in some cases^{11,24,50,51} suggesting that top-down factors such as
384 attention may also potentially enhance coherence by altering neuronal sensitivity in a similar
385 manner. Moreover, factors such as noise-level and size of stimulus have been shown to alter the
386 spatial scale of LFP leading to more spatially tuned gamma activity^{29,30,52}. In such cases, changes
387 in coherence can also come about more directly from an increase or decrease in rhythmic
388 synaptic input to neurons regardless of their activation-level. Quantitative analyses using an
389 approach similar to ours will be necessary to clarify the mechanistic origins of rate-independent
390 changes in coherence.

391 The potential implications of gating coherence based on activation-level are at least
392 twofold. First as we have shown, this would lead to a similarity in the spatial resolution of firing
393 rate and gamma synchrony codes. It has been argued that the brain can decode temporally
394 multiplexed codes using known mechanisms⁴ such as synaptic depression and facilitation that
395 endow neurons with multiple synaptic timescales^{53,54}. Performing spatial de-multiplexing in
396 addition to the above would not be as easy because it would require differential spatial pooling
397 depending on the timescale. Moreover it is unclear if such algorithms might be supported by the
398 brain's neural hardware. The proposed mechanism obviates the need to deal with such
399 complexities by matching the spatial scales of the two codes. Second, current theories suggest
400 that gamma synchrony may be involved in the encoding of sensory information⁵⁵⁻⁵⁷, regulating
401 information flow between brain areas⁵⁸⁻⁶⁰, and facilitating synaptic plasticity^{6,61,62}. Supporting
402 such a diverse range of functions would require synchrony to be robust to the precise level of
403 neuronal activity. Adaptive gating of coherence based on activation-level would also help
404 achieve this by preserving the transfer of synchrony in the face of elevated asynchronous
405 background activity.

406 **Methods**

407 **M1 Electrophysiological recordings**

408 Two adult male rhesus monkeys (*Macaca mulatta*) D98 and F03 weighing 16 kg and 11 kg
409 respectively, took part in the experiments. Cranial headposts and form-specific chambers were
410 surgically implanted. Recording chambers were positioned stereotactically over the operculum in
411 area V1 in both hemispheres of D98 and right hemisphere of F03 with the aid of high-resolution
412 anatomical scans. Skull parameters extracted from these scans were used for designing the
413 headpost and the recording chambers to fit the skull surface. A more detailed description of these
414 methods can be found elsewhere⁶³⁻⁶⁵. A custom-built array of tetrodes⁶⁶ was chronically
415 implanted in area V1 inside the recording chamber implanted in the left hemisphere of the
416 monkey D98. The tetrodes were at least 200 μ m apart⁶⁷. Recordings were also carried out non-
417 chronically from the right hemisphere of both monkeys. In these sessions, one to four manually
418 adjustable microdrives (Crist Instrument Co.) were inserted into a custom-built grid and the
419 activity was recorded using tetrodes. The experimental and surgical procedures were performed
420 with great care and in full compliance with the German Law for the Protection of Animals, the
421 European Community guidelines for the care and use of laboratory animals (EUVS
422 86/609/EEC), and the recommendations of Weatherall report⁶⁸. The regional authorities
423 (Regierungspräsidium Tuebingen) approved our experimental protocol application and the
424 institutional representatives for animal protection supervised all procedures.

425 The raw voltage signal was passed through an analog bandpass filter (1-475 Hz), sampled
426 at \sim 1990.7 Hz, digitized (12 bits) and stored as the LFP signal. Multiunit spikes were identified
427 by passing the raw signal through a separate analog bandpass filter (600 Hz-6 KHz), followed by
428 sampling (32 KHz), digitization (12 bits) and detecting the times at which the signal crosses a
429 predefined threshold (25 μ V). Following each threshold crossing, a segment of 32 samples (1ms)
430 was extracted from all four channels of the tetrode and these waveforms were stored for offline
431 clustering. Single-unit spikes were then isolated from multiunit activity by a custom-built
432 clustering software⁶⁶ that uses features extracted from the stored multiunit spike waveforms.

433 **M2 Visual stimuli**

434 A dedicated graphics workstation (TDZ 2000; Intergraph Systems) running an OpenGL-based
435 program was used for rendering visual stimuli, while the behavioral aspects (e.g. juice reward,
436 trial abortion) were controlled using the QNX real-time operating system (QNX Software
437 Systems Ltd). The display system comprised of a custom-made mirror stereoscope with an LCD
438 monitor (resolution of 1024x768; refresh rate of 60 Hz) on each side as shown in **Fig. 1B**, and
439 allowed for dichoptic presentation of stimuli.

440 Each session began with a calibration procedure⁶³ to ensure that the monkeys could
441 correctly overlay (fuse) the central fixation markers (0.2°) on the two displays. The following
442 procedure was then carried out to determine the position and orientations of the stimuli to be
443 used in the experiments. A grating of arbitrary orientation was presented binocularly (i.e., shown
444 to both eyes) at a parafoveal location while the monkey fixated on the central marker. The
445 location, size and orientation of the grating are then systematically changed until the location of
446 the receptive field and the orientation preference of the multiunit response could be estimated.
447 Such online estimation was made possible by playing the multiunit activity through a sound
448 amplifier (Grass Technologies). The pair of orthogonal orientations (θ_A and θ_B) that elicited
449 maximal differential multiunit response were identified and used in the experiment.

450 Each trial of the experiment began with the monkey fixating on a central marker (0.2°).
451 After maintaining fixation for 300ms, a static sine-wave grating stimulus (diameter of 1-2°;

452 spatial frequency of 3-5 cycles/deg; contrast 70%) of two possible orientations was displayed
453 monocularly to one of the eyes for a period of one second (**Fig. 1B**). The animal was required to
454 maintain fixation within a circular window with a radius 0.5° from the center of the marker
455 throughout the duration of the trial. At the end of each successful trial, a drop of apple juice was
456 delivered as a reward. A failure resulted in abortion of the trial without reward. Depending on the
457 orientation of the grating and eye of presentation, each trial belonged to one of four stimulus
458 conditions (**Fig. 1B**). A typical recording session included 200 trials of each condition.
459 Throughout this paper, the term ‘preferred’ orientation (eye) is used to refer to the orientation
460 (eye) that elicits higher firing rate for a given singleunit. The complementary condition is dubbed
461 ‘nonpreferred’.

462 **M3 Data Analysis**

463 Singleunits were first tested for visual responsiveness by comparing stimulus-evoked firing rates
464 to baseline. Only neurons that exhibited a significant increase in their firing rates in response to
465 visual stimulus ($p < 0.05$; Wilcoxon rank-sum test) were considered for further analyses. Unless
466 otherwise specified, all time-domain and spectral estimates were based on responses recorded
467 between 400-1000ms following stimulus onset when signals were relatively more stationary.

468 ***Spike-field coherence (SFC)***

469 To measure the extent of rhythmic synchronization between LFP and spike trains at all
470 frequencies, we estimated spike-field coherence (SFC) defined as the squared magnitude of the
471 cross-spectrum divided by the product of the auto-spectra⁶⁹:

$$C(f) = \frac{|S_{xy}(f)|^2}{S_{xx}(f)S_{yy}(f)} \quad (1)$$

472 where $C(f)$ denotes the spike-field coherence at frequency f , $S_{xy}(f)$ denotes the cross-spectral
473 density function between spike train x and LFP signal y , $S_{xx}(f)$ and $S_{yy}(f)$ are the respective
474 autospectra. All spectral estimates were carried out using multi-taper method with $K = 7$
475 orthogonal Slepian tapers w_k to yield spectral smoothing of approximately ± 4 Hz at a frequency
476 resolution of ~ 1 Hz. This involved multiplying each data sequence \mathbf{x}_n (\mathbf{y}_n for LFP) with the
477 different tapers to obtain K independent spectral estimates and then averaging them:

$$X_k^n(f) = \sum_{t=1}^T w_k(t) \cdot x_n(t) e^{-j2\pi ft}$$
$$S_{xx}(f) = \frac{1}{NK} \sum_{n=1}^N \sum_{k=1}^K X_k^n(f) \cdot X_k^{n*}(f)$$

478 where $X_k^n(f)$ denotes the k^{th} Slepian-tapered Fourier transform of \mathbf{x}_n , $X_k^{n*}(f)$ its complex
479 conjugate, N is the total number of trials, and T is the duration of the signals x and y .

480 ***Significance test for SFC***

481 To test the statistical significance of SFC for each spike-LFP pair at every frequency, we
482 obtained multiple estimates of SFCs by shuffling the order of the trials of spike trains thereby
483 destroying the phase relationship between spike trains and LFPs. At any given frequency, the

484 estimated value of SFC before shuffling was deemed to be significant if the probability of
485 drawing it from the distribution of shuffled SFC estimates was less than 0.01. Only those pairs
486 which showed significant SFC at 8 consecutive bins (~8Hz) in the frequency range between 30-
487 45 Hz in at least one of the stimulus conditions were considered for further analyses. We
488 assessed the significance of difference in SFC across the two pairs of conditions by a shuffling
489 procedure similar to the one described above. Trials from the two conditions to be tested were
490 pooled together. Half the trials were then dubbed to be from one condition, while the other half
491 were labeled to be from the other condition. SFCs were then estimated for the two conditions and
492 the differences in SFCs were computed. This procedure was repeated several times and the true
493 difference was compared against the distribution of 'fake' differences ($p < 0.01$). A similar
494 technique was used to assess significance of modulations in gamma-band LFP power. Statistical
495 significance of firing rate changes were tested using two-sided Wilcoxon rank-sum test ($p = 0.05$)
496 by comparing spike counts across trials for the relevant stimulus conditions.

497 **Modulation Indices**

498 Orientation and ocularity preferences were first determined for each neuron by estimating rate-
499 modulation indices (M_R) derived from the average firing rates (R) elicited by the pair of stimuli:

$$M_R = \frac{R_A - R_B}{R_A + R_B} \quad (2)$$

500 Here A and B are used as placeholders to denote the pair of conditions that correspond to the
501 presentation of, either the pair of orthogonal gratings to the neuron's preferred eye (orientation
502 preference), or the preferred orientation to the right and left eye (ocularity preference). Similar
503 definitions were used for quantifying modulations in the gamma-band LFP power (M_L) and
504 gamma-band spike-field coherence (M_C). To explicitly test whether modulations in firing rate
505 (M_R) or LFP power (M_L) better predicted modulations in neuronal synchrony (M_C), we
506 performed multiple linear regression $M_C = \beta_R M_R + \beta_L M_L + \beta_0$ to determine coefficients β_R and
507 β_L on predictors M_R and M_L respectively, according to:

$$\boldsymbol{\beta} = (\mathbf{M}^T \mathbf{M})^{-1} (\mathbf{M}^T \mathbf{M}_C) \quad (3)$$

508 where $\boldsymbol{\beta} = (\beta_R \ \beta_L \ \beta_0)^T$, and $\mathbf{M} = (\mathbf{M}_R \ \mathbf{M}_L \ \mathbf{1})$ where \mathbf{M}_R and \mathbf{M}_L denote vectors of
509 modulation indices across the population. To compare the quality of predictions given by M_R and
510 M_L , we regressed M_C against M_R and M_L separately. The mean slopes of both regressions were
511 used individually to generate predictions \widetilde{M}_C . For each spike-LFP pair, normalised residuals were
512 then estimated by computing the squared deviation of the prediction from the experimental
513 measurement M_C , normalized by the variance of the measurement: $(\widetilde{M}_C - M_C)^2 / \langle (\delta M_C)^2 \rangle$.

514 **Pseudo spike-field coherence**

515 In addition to assessing modulation of firing rates and SFC across conditions, we directly tested
516 whether firing rates exhibited correlated variability with SFCs across trials within a given
517 condition. This was done by calculating the Spearman correlation coefficient (ρ) between spike
518 count across trials and single-trial coherence estimates. Coherence estimates for individual trials
519 were obtained through the following procedure⁵. For any given trial, the z-transform of the SFC
520 estimated by leaving out that trial, was subtracted from the original z-transformed SFC estimate
521 after weighting each term with the number of trials used in the estimate:

$$q_i(f) = N \cdot q(f) - (N - 1) q^i(f) \quad (4)$$

522 where $q_i(f)$ denotes pseudo-coherence of the i^{th} trial, $q(f)$ is the coherence across all N trials,
523 and $q^i(f)$ is coherence estimated by leaving the i^{th} trial out. Here $q = \sqrt{-2(K-1) \log(1-C)}$
524 denotes the z-transformed value of the estimated coherence C with $K = 7$ tapers.

525 ***Spike-triggered LFP***

526 For each neuron, spike-triggered average (STA) of the LFP was estimated first by averaging
527 300ms segments around the time of each spike emitted by that neuron. The result was divided by
528 the standard deviation of the LFP to obtain normalised STA²². The peak amplitude of the
529 normalised STA was taken as a measure of the correlation between LFP and neuronal membrane
530 potential. To determine whether LFP was robustly correlated with the membrane potential across
531 all stimulus conditions, normalised STAs were computed separately for each stimulus condition
532 and their peak amplitudes were compared.

533 ***Correction procedures***

534 To ensure that our test statistics are not affected by differences in bias and variance across
535 conditions, we took the following measures to avoid potential confounds in SFC estimation.
536 Each condition included the same number of trials and the lengths of data segments in all trials
537 were identical across conditions. For each single-unit, SFCs were calculated between its spike
538 trains and concurrently recorded LFPs from all tetrodes. Consequently $\sim 70\%$ of SFCs (275/400
539 pairs) were obtained from spikes and LFPs belonging to different electrodes. Furthermore, when
540 using spikes and LFP from the same electrode, a 4ms segment of LFP was removed around the
541 time of each spike and those data points were replaced using cubic spline interpolation. This
542 procedure resulted in a significant reduction of SFC, but only in the frequency range above 100
543 Hz (**Supplementary Fig. 13**) implying that gamma-band SFC was not affected by spurious
544 correlations between spikes and LFP. Therefore, we retained the spike-LFP pairs for which
545 spikes and LFP were recorded on the same electrode in order to gain statistical power.

546 **M4 Neuronal model**

547 Rhythmic spiking process $r(t)$ was modeled as a sum of asynchronous excitation $A(t)$ with
548 mean a and rhythmic input $\psi(t)$ as described in the results. The net excitability due to $\psi(t)$ is
549 assumed to be zero, so the mean activity is given by $\langle r(t) \rangle = \langle A(t) \rangle = a$. Variability on the
550 other hand, is inherited from both inputs according to:

$$\langle (\delta \mathbf{r})^2 \rangle_t = \langle (\delta \mathbf{A})^2 \rangle_t + g^2 \langle (\delta \Psi)^2 \rangle_t \quad (5)$$

551 where functions of time are denoted using boldface letters for convenience, g is the sensitivity to
552 synchronous input, and subscript $\langle \cdot \rangle_t$ denotes expectation over time. To estimate $\langle (\delta \mathbf{r})^2 \rangle_t$, we
553 first time-shifted the spike train of each trial i by an amount δt_i so that gamma phases of the
554 simultaneously recorded LFP traces were aligned across trials, and then computed the temporal
555 variability of the trace obtained by averaging the resulting spike trains across trials
556 (**Supplementary Fig. 7A – top right**). We isolated the component of variability due to rhythmic
557 input by subtracting the asynchronous component $\langle (\delta \mathbf{A})^2 \rangle_t$ from $\langle (\delta \mathbf{r})^2 \rangle_t$. The asynchronous
558 component was estimated by a procedure in which elements of $\{\delta t_i\}$ were shuffled before
559 shifting the spike trains. This shuffling procedure essentially randomizes the phases of gamma
560 cycles of different trials, so that any temporal variability in the resulting trial-averaged firing
561 rates will be solely due to asynchronous dynamics of the spiking process (**Supplementary Fig.**
562 **7A – bottom left**). The shuffling procedure was carried out several times and the mean of the

563 resulting distribution of variabilities $\langle(\delta\mathbf{r})^2\rangle_t^{shuffled}$ was used as an estimate of $\langle(\delta\mathbf{A})^2\rangle_t$.
564 Neuronal sensitivity g was then estimated according to:

$$g = \sqrt{\frac{\langle(\delta\mathbf{r})^2\rangle_t - \langle(\delta\mathbf{r})^2\rangle_t^{shuffled}}{\langle(\delta\Psi)^2\rangle_t}} \quad (6)$$

565 where $\langle(\delta\mathbf{r})^2\rangle_t^{shuffled}$ denotes variability estimated through the shuffling procedure.

566 Acknowledgements

567 We would like to thank Drs. Jacob Macke, Philipp Berens, Esther Florin, and David Omer for
568 comments on previous versions of the manuscript. This work was supported by the Max-Planck
569 Society and the German Federal Ministry of Education and Research (BMBF; FKZ: 01GQ1002).

570 References

- 571 1. Shadlen, M. N. & Newsome, W. T. Noise, neural codes and cortical organization. *Curr.*
572 *Opin. Neurobiol.* **4**, 569–579 (1994).
- 573 2. Eggermont, J. J. Is there a neural code? *Neurosci. Biobehav. Rev.* **22**, 355–370 (1998).
- 574 3. Butts, D. A. *et al.* Temporal precision in the neural code and the timescales of natural
575 vision. *Nature* **449**, 92–95 (2007).
- 576 4. Panzeri, S., Brunel, N., Logothetis, N. K. & Kayser, C. Sensory neural codes using
577 multiplexed temporal scales. *Trends Neurosci.* **33**, 111–120 (2010).
- 578 5. Womelsdorf, T., Fries, P., Mitra, P. P. & Desimone, R. Gamma-band synchronization in
579 visual cortex predicts speed of change detection. *Nature* **439**, 733–736 (2006).
- 580 6. Vinck, M. *et al.* Gamma-phase shifting in awake monkey visual cortex. *J. Neurosci.* **30**,
581 1250–7 (2010).
- 582 7. Sridharan, D., Boahen, K. & Knudsen, E. I. Space coding by gamma oscillations in the
583 barn owl optic tectum. *J. Neurophysiol.* **105**, 2005–2017 (2011).
- 584 8. Fries, P., Reynolds, J. H., Rorie, A. E. & Desimone, R. Modulation of Oscillatory
585 Neuronal Synchronization by Selective Visual Attention. *Science (80-.)*. **291**, 1560–1563
586 (2001).
- 587 9. Lakatos, P., Karmos, G., Mehta, A. D., Ulbert, I. & Schroeder, C. E. Entrainment of
588 neuronal oscillations as a mechanism of attentional selection. *Science* **320**, 110–3 (2008).
- 589 10. Fries, P., Roelfsema, P. R., Engel, A. K., König, P. & Singer, W. Synchronization of
590 oscillatory responses in visual cortex correlates with perception in interocular rivalry.
591 *Proc. Natl. Acad. Sci. U. S. A.* **94**, 12699–12704 (1997).
- 592 11. Fries, P., Jan-Hinrich, Roelfsema, P. R., Singer, W. & Engel, A. K. Oscillatory neuronal
593 synchronization in primary visual cortex as a correlate of stimulus selection. *J. Neurosci.*
594 **22**, 3739–3754 (2002).
- 595 12. Pesaran, B., Pezaris, J. S., Sahani, M., Mitra, P. P. & Andersen, R. A. Temporal structure
596 in neuronal activity during working memory in Macaque parietal cortex. *Nature* **8336**,
597 805–811 (2002).
- 598 13. Colgin, L. L. & Moser, E. I. Gamma oscillations in the hippocampus. *Physiol. Bethesda*
599 *Md* **25**, 319–329 (2010).
- 600 14. Hammond, C., Bergman, H. & Brown, P. Pathological synchronization in Parkinson’s
601 disease: networks, models and treatments. *Trends Neurosci.* **30**, 357–364 (2007).
- 602 15. Gonzalez-Burgos, G. & Lewis, D. A. GABA Neurons and the Mechanisms of Network

- 603 Oscillations: Implications for Understanding Cortical Dysfunction in Schizophrenia.
604 *Schizophr. Bull.* **34**, 944–961 (2008).
- 605 16. Bartos, M., Vida, I. & Jonas, P. Synaptic mechanisms of synchronized gamma oscillations
606 in inhibitory interneuron networks. *Nat. Rev. Neurosci.* **8**, 45–56 (2007).
- 607 17. Buzsáki, G. & Wang, X.-J. Mechanisms of gamma oscillations. *Annu. Rev. Neurosci.* **35**,
608 203–225 (2012).
- 609 18. Einevoll, G. T., Kayser, C., Logothetis, N. K. & Panzeri, S. Modelling and analysis of
610 local field potentials for studying the function of cortical circuits. *Nat. Rev. Neurosci.* **14**,
611 770–85 (2013).
- 612 19. Buzsáki, G., Anastassiou, C. A. & Koch, C. The origin of extracellular fields and currents
613 — EEG, ECoG, LFP and spikes. *Nat. Rev. Neurosci.* **13**, 407–420 (2012).
- 614 20. Haider, B., Schulz, D. P. P. A., Häusser, M. & Carandini, M. Millisecond Coupling of
615 Local Field Potentials to Synaptic Currents in the Awake Visual Cortex. *Neuron* **90**, 35–
616 42 (2016).
- 617 21. Berens, P., Keliris, G. A., Ecker, A. S., Logothetis, N. K. & Tolias, A. S. Comparing the
618 Feature Selectivity of the Gamma-Band of the Local Field Potential and the Underlying
619 Spiking Activity in Primate Visual Cortex. *Front. Syst. Neurosci.* **2**, 11 (2008).
- 620 22. Okun, M., Naim, A. & Lampl, I. The subthreshold relation between cortical local field
621 potential and neuronal firing unveiled by intracellular recordings in awake rats. *J.*
622 *Neurosci.* **30**, 4440–4448 (2010).
- 623 23. Riehle, A., Grün, S., Diesmann, M. & Aertsen, A. Spike synchronization and rate
624 modulation differentially involved in motor cortical function. *Science* **278**, 1950–1953
625 (1997).
- 626 24. Biederlack, J. *et al.* Brightness Induction: Rate Enhancement and Neuronal
627 Synchronization as Complementary Codes. *Neuron* **52**, 1073–1083 (2006).
- 628 25. Li, A., Gire, D. H. & Restrepo, D. Spike-Field Coherence in a Population of Olfactory
629 Bulb Neurons Differentiates between Odors Irrespective of Associated Outcome. *J.*
630 *Neurosci.* **35**, 5808–5822 (2015).
- 631 26. Niessing, J. *et al.* Hemodynamic signals correlate tightly with synchronized gamma
632 oscillations. *Science* **309**, 948–951 (2005).
- 633 27. Viswanathan, A. & Freeman, R. D. Neurometabolic coupling in cerebral cortex reflects
634 synaptic more than spiking activity. *Nat. Neurosci.* **10**, 1308–1312 (2007).
- 635 28. Markowitz, D. A., Collman, F., Brody, C. D., Hopfield, J. J. & Tank, D. W. Rate-specific
636 synchrony: using noisy oscillations to detect equally active neurons. *Proc. Natl. Acad. Sci.*
637 *U. S. A.* **105**, 8422–8427 (2008).
- 638 29. Jia, X., Smith, M. A. & Kohn, A. Stimulus selectivity and spatial coherence of gamma
639 components of the local field potential. *J. Neurosci.* **31**, 9390–9403 (2011).
- 640 30. Jia, X., Tanabe, S. & Kohn, A. Gamma and the coordination of spiking activity in early
641 visual cortex. *Neuron* **77**, 762–74 (2013).
- 642 31. Bartfeld, E. & Grinvald, A. Relationships between orientation-preference pinwheels,
643 cytochrome oxidase blobs, and ocular-dominance columns in primate striate cortex. *Proc.*
644 *Natl. Acad. Sci. U. S. A.* **89**, 11905–9 (1992).
- 645 32. Blasdel, G. G. Differential Imaging of Ocular Dominance and Orientation Selectivity in
646 Monkey Striate Cortex. *J. Neurosci.* **12**, 3115–38 (1992).
- 647 33. Azouz, R. & Gray, C. M. Dynamic spike threshold reveals a mechanism for synaptic
648 coincidence detection in cortical neurons in vivo. *Proc. Natl. Acad. Sci. U. S. A.* **97**, 8110–

- 649 8115 (2000).
- 650 34. Henze, D. A. & Buzsáki, G. Action potential threshold of hippocampal pyramidal cells in
651 vivo is increased by recent spiking activity. *Neuroscience* **105**, 121–130 (2001).
- 652 35. Azouz, R. & Gray, C. M. Adaptive coincidence detection and dynamic gain control in
653 visual cortical neurons in vivo. *Neuron* **37**, 513–523 (2003).
- 654 36. Wilent, W. B. & Contreras, D. Stimulus-dependent changes in spike threshold enhance
655 feature selectivity in rat barrel cortex neurons. *J. Neurosci.* **25**, 2983–2991 (2005).
- 656 37. Cardin, J. A., Kumbhani, R. D., Contreras, D. & Palmer, L. A. Cellular mechanisms of
657 temporal sensitivity in visual cortex neurons. *J. Neurosci.* **30**, 3652–3662 (2010).
- 658 38. Bernander, O., Douglas, R. J., Martin, K. A. & Koch, C. Synaptic background activity
659 influences spatiotemporal integration in single pyramidal cells. *Proc. Natl. Acad. Sci. U.*
660 *S. A.* **88**, 11569–11573 (1991).
- 661 39. Marsálek, P., Koch, C. & Maunsell, J. On the relationship between synaptic input and
662 spike output jitter in individual neurons. *Proc. Natl. Acad. Sci. U. S. A.* **94**, 735–740
663 (1997).
- 664 40. Rudolph, M. & Destexhe, A. Tuning neocortical pyramidal neurons between integrators
665 and coincidence detectors. *J. Comput. Neurosci.* **14**, 239–251 (2003).
- 666 41. Prescott, S. A., Ratté, S., De Koninck, Y. & Sejnowski, T. J. Nonlinear interaction
667 between shunting and adaptation controls a switch between integration and coincidence
668 detection in pyramidal neurons. *J. Neurosci.* **26**, 9084–9097 (2006).
- 669 42. Ratte, S., Hong, S., DeSchutter, E. & Prescott, S. A. Impact of neuronal properties on
670 network coding: Roles of spike initiation dynamics and robust synchrony transfer. *Neuron*
671 **78**, 758–772 (2013).
- 672 43. Perrenoud, Q., Pennartz, C. M. A. & Gentet, L. J. Membrane Potential Dynamics of
673 Spontaneous and Visually Evoked Gamma Activity in V1 of Awake Mice. *PLoS Biol.* **14**,
674 (2016).
- 675 44. Ray, S., Ni, A. M. & Maunsell, J. H. R. Strength of Gamma Rhythm Depends on
676 Normalization. *PLoS Biol.* **11**, (2013).
- 677 45. Ray, S., Crone, N. E., Niebur, E., Franaszczuk, P. J. & Hsiao, S. S. Neural correlates of
678 high-gamma oscillations (60–200 Hz) in macaque local field potentials and their potential
679 implications in electrocorticography. *J. Neurosci.* **28**, 11526–11536 (2008).
- 680 46. Fries, P., Womelsdorf, T., Oostenveld, R. & Desimone, R. The effects of visual
681 stimulation and selective visual attention on rhythmic neuronal synchronization in
682 macaque area V4. *J. Neurosci.* **28**, 4823–4835 (2008).
- 683 47. Lepage, K. & Kramer, M. Dependence of Spike-Field Coherence on expected intensity.
684 *Neural Comput.* (2011).
- 685 48. Lepage, K. Q. *et al.* A procedure for testing across-condition rhythmic spike-field
686 association change. *J Neurosci Methods* **213**, 43–62 (2013).
- 687 49. De La Rocha, J., Doiron, B., Shea-Brown, E., Josić, K. & Reyes, A. Correlation between
688 neural spike trains increases with firing rate. *Nature* **448**, 802–806 (2007).
- 689 50. Chalk, M. *et al.* Attention Reduces Stimulus-Driven Gamma Frequency Oscillations and
690 Spike Field Coherence in V1. *Neuron* **66**, 114–125 (2010).
- 691 51. Wang, Y., Iliescu, B. F., Ma, J., Josic, K. & Dragoi, V. Adaptive changes in neuronal
692 synchronization in macaque v4. *J. Neurosci.* **31**, 13204–13213 (2011).
- 693 52. Ray, S. & Maunsell, J. H. R. Differences in Gamma Frequencies across Visual Cortex
694 Restrict Their Possible Use in Computation. *Neuron* **67**, 885–896 (2010).

- 695 53. Salinas, E. & Sejnowski, T. J. Correlated neuronal activity and the flow of neural
696 information. *Nat. Rev. Neurosci.* **2**, 539–50 (2001).
- 697 54. Izhikevich, E. M., Desai, N. S., Walcott, E. C. & Hoppensteadt, F. C. Bursts as a unit of
698 neural information: Selective communication via resonance. *Trends Neurosci.* **26**, 161–
699 167 (2003).
- 700 55. König, P., Engel, A. K., Roelfsema, P. R. & Singer, W. How precise is neuronal
701 synchronization? *Neural Comput.* **7**, 469–485 (1995).
- 702 56. Sejnowski, T. J. & Paulsen, O. Network oscillations: emerging computational principles.
703 *J. Neurosci.* **26**, 1673–1676 (2006).
- 704 57. Fries, P., Nikolić, D. & Singer, W. The gamma cycle. *Trends Neurosci.* **30**, 309–316
705 (2007).
- 706 58. Fries, P. A mechanism for cognitive dynamics: neuronal communication through neuronal
707 coherence. *Trends Cogn. Sci.* **9**, 474–80 (2005).
- 708 59. Womelsdorf, T. *et al.* Modulation of neuronal interactions through neuronal
709 synchronization. *Science* **316**, 1609–12 (2007).
- 710 60. Colgin, L. L. *et al.* Frequency of gamma oscillations routes flow of information in the
711 hippocampus. *Nature* **462**, 353–357 (2009).
- 712 61. Wespapat, V., Tegnigkeit, F. & Singer, W. Phase sensitivity of synaptic modifications in
713 oscillating cells of rat visual cortex. *J. Neurosci.* **24**, 9067–9075 (2004).
- 714 62. Buzsáki, G. *Rhythms of the Brain. Rhythm. Brain* **1**, (Oxford Univ. Press, 2006).
- 715 63. Keliris, G. A., Logothetis, N. K. & Tolias, A. S. The role of the primary visual cortex in
716 perceptual suppression of salient visual stimuli. *J. Neurosci.* **30**, 12353–12365 (2010).
- 717 64. Logothetis, N. K., Guggenberger, H., Peled, S. & Pauls, J. Functional imaging of the
718 monkey brain. *Nat. Neurosci.* **2**, 555–562 (1999).
- 719 65. Logothetis, N. K., Merkle, H., Augath, M., Trinath, T. & Ugurbil, K. Ultra-High
720 Resolution fMRI in Monkeys with Implanted RF Coils. *J Neurosci Methods* **35**, 227–242
721 (2002).
- 722 66. Tolias, A. S. *et al.* Recording chronically from the same neurons in awake, behaving
723 primates. *J. Neurophysiol.* **98**, 3780–90 (2007).
- 724 67. Ecker, A. S. *et al.* Decorrelated neuronal firing in cortical microcircuits. *Science* **327**,
725 584–587 (2010).
- 726 68. Weatherall report. The use of non-human primates in research. 1–153 (2006).
- 727 69. Bendat, J. S. & Piersol, A. G. *Random data. Consultant* (Wiley, 1986).
- 728